2-D Localization, Angular Separation and Vital Signs Monitoring Using a SISO FMCW Radar for Smart Long-Term Health Monitoring Environments

2-D Localization, Angular Separation and Vital Signs Monitoring Using a SISO FMCW Radar for Smart Long-term Health Monitoring Environments

Marco Mercuri, Giulia Sacco, *Student Member, IEEE,* Rainer Hornung, Peng Zhang, Huib Visser, Martijn Hijdra, Yao-Hong Liu, *Senior Member, IEEE,* Stefano Pisa, *Senior Member, IEEE,* Barend van Liempd, and Tom Torfs

***Abstract*—A single-input and single-output (SISO) frequency-modulated continuous wave (FMCW) radar architecture is proposed and *in vivo* demonstrated for remote two-dimensional (2-D) localization (range and angular information) and vital signs monitoring of multiple subjects. The radar sensor integrates two frequency scanning antennas which allow angular separation and enable determining a 2-D map (range vs. angle) of a room environment from which people can be distinguished from objects and clutter. After technical tests to validate the functionality of the proposed architecture and data processing algorithm, a practical setup was successfully demonstrated to locate human volunteers, at different absolute distances and orientations, and to retrieve their respiratory and heart rate information. Experimental results show that this radar sensor can monitor accurately the vital signs of multiple subjects within typical room settings, reporting maximum mean absolute errors of 0.747 breaths-per-minute and 2.645 beats-per-minute respectively for respiration rate and heartbeat. Practical applications arise for Internet of Things (IoT), ambient assisted living, healthcare, geriatric and quarantine medicine, automotive, rescue and security purposes.**

***Index Terms*—2-D localization, angular separation, biomedical applications, contactless, Doppler, frequency-modulated continuous wave (FMCW), Internet of Things (IoT) system architecture, rampart antenna, remote radar sensing, single-input and single-output (SISO) radar, vital signs monitoring.**

I. Introduction

RADAR represents an emerging key technology for healthcare and Internet of Things (IoT) to provide benefits for diagnosis, long-term monitoring and detection of emergency situations, as they can remotely measure heartbeat and respiration, speed, and distance of multiple individuals [1]–[3]. Radar systems can operate at many frequencies, varying from a few MHz to optical frequencies. However, a major advantage of radio-frequency (RF) and millimeter waves (mm-wave) architectures is that they guarantee both the optimal resolution and sensitivity to remotely monitor human targets in a home environment, thus representing the most suitable solution for applications like localization and vital signs monitoring (measure of heartbeat and respiration rate) [4], [5]. For localization, and hence to have a proper radar range resolution, it is important to transmit signals of a certain bandwidth [6]. The wider the band is, the finer is the range resolution. Considering the typical sizes of human individuals, it is normally required a range resolution of 15-60 cm [7]. This corresponds to bandwidths of 1 GHz and 0.25 GHz, respectively. At RF and mm-wave frequencies, there are many sufficiently wide bands designated for unlicensed operation. On the other hand, for vital signs monitoring, it is fundamental the operating frequency. The higher it is, the higher is the sensitivity in detecting sub-millimeter motions as the ones caused by the cardiopulmonary activity [8]. Sub-10GHz (i.e., RF) radars have both a sufficient sensitivity in detecting vital signs and a sufficient bandwidth for localization [9], [10], therefore they are good candidates for people monitoring. Moreover, they present lower phase noise and pathloss than the mm-wave solutions. In fact, they can monitor subjects at long distances (several meters) even through clothes, blankets, and many barriers (e.g. glass, doors or walls) [11], [12]. Furthermore, they can also operate in totally dark environments and in smoke-filled areas. All these features allow the use of this technology in many practical applications of strong interest, such as monitoring people lying on their beds in the hospital, elderly people in nursing home, people during a meeting in a room, watching TV or playing videogames, etc., as well as detecting potential emergency situations such as cardiovascular diseases, lung diseases, sudden infant death syndrome (SIDS), apnea and fall incidents [4], [13]–[16]. The monitoring can be performed continuously while preserving the privacy of the subjects and without health effects. This paves the way of future smart long-term monitoring environments by evolving to automated nurse call solutions [1], allowing achieving the goals of remotely monitoring the well-being of people, enlarging the period of aged persons of living in their familiar home environment, prompt emergencies detection and immediate medical attention [17]–[19]. The possibility of contactless monitoring is a hot topic especially for those applications where wearable medical devices cannot be used (e.g., patients with severe and extensive burn wounds) or create discomfort and are unpleasant for long-term use (e.g., while sleeping, showering, normal daily activities) [20]. Radar systems are

M. Mercuri, R. Hornung, P. Zhang, M. Hijdra, H. Visser and Y-H. Liu are with imec - Netherlands, 5656 AE Eindhoven, The Netherlands (e-mail: marco.mercuri@imec.nl; rainer.hornung@imec.nl; peng.zhang@imec.nl; huib.visser@imec.nl; martijn.hijdra@imec.nl; yao-hong.liu@imec.nl).

G. Sacco was with imec - Netherlands, 5656 AE Eindhoven, The Netherlands, and currently with the Department of Information Engineering, Electronics and Telecommunication of Sapienza University of Rome, Rome, Italy (e-mail: giulia.sacco@uniroma1.it).

S. Pisa is with the Department of Information Engineering, Electronics and Telecommunication of Sapienza University of Rome, Rome, Italy (e-mail: stefano.pisa@uniroma1.it).

B. van Liempd and T. Torfs are with imec, Leuven 3001, Belgium (e-mail: barend.vanliempd@imec.be; tom.torfs@imec.be).

Manuscript received September 24, 2020.

ideal in situations with risk of infection or pandemics (e.g., COVID-19 crisis) to remotely monitor household members in quarantine or in hospitals (e.g., departments of infectious diseases) to reduce contamination risks, but also to detect whether people in spaces are respecting social distancing. The range of applications is even beyond medical. This technology can be applied in other fields such as ambient light and temperature smart control, driver monitoring as additional step towards autonomous vehicles, surveillance or for search and rescue situations to detect people in smoke-filled areas or underneath collapsed buildings [11], [12], [21], [22].

In the last two decades, a lot of research was conducted aiming at long-term health monitoring and in particular at remote people localization and vital signs sensing. Continuous wave (CW) radars have been proposed for vital signs monitoring of a single person with the limitation that any information about his/her position cannot be provided [23]–[31]. Ultra-wideband (UWB) single-input and single-output (SISO) radars based on stepped-frequency continuous wave (SFCW), frequency-modulated continuous wave (FMCW), frequency shift keying (FSK), and ultra-wideband impulse-radio (UWB-IR) architectures offer, instead, the possibility of determining the absolute distances (range information) and the vital signs parameters of multiple subjects only if they are in different range bins [7], [32]–[44]. In fact, the main limitation is that these solutions cannot provide azimuth information and, hence, they cannot resolve targets in the angular dimension. In order to tackle that and, therefore, allowing 2-D (two-dimensional) localization, namely providing range and azimuth information, multiple-input and multiple-output (MIMO) UWB radars have been proposed [45]–[49]. Obviously, as opposite to SISO architectures, MIMO radars require an array of radiators and consequently multiple transmitters and receivers. This involves higher power consumption, larger silicon's area, complex design and control, and higher amount of data to be processed. Similar drawbacks are experienced by electrical beam-steering radar sensors which have been also investigated for 2-D localization and vital signs monitoring [50], [51]. This architecture in fact requires arrays of antennas and time-delay or phase shifter units (or a combination of them) to steer the beam in the desired direction [50]–[52]. In addition, pointing to only one direction per time (hence covering only a limited area), the beam should scan quite fast the whole monitored environment to aim at the targets (which are at different locations) such that their Doppler signals can be extracted satisfying the Nyquist theorem. Therefore, a first group of waveforms should be transmitted to point the beam to one direction, then another group (with different phase shifts and/or time delays) is sent to steer it to a different one, and so on to cover the whole environment. This operation requires hence a short pulse repetition interval (PRI) among the groups. It should be specified that transmitting multiple waveforms (as for MIMO and beam-steering radars) involves a trade-off between radiated power and PRI in order to satisfy the UWB spectral mask requirements [10]. Since the PRI cannot be increased too much (to avoid violating the Nyquist theorem when extracting the Doppler signals), the transmitted power should be decreased. However, this reduces inevitably the signal-to-noise ratio (SNR). For example, a 250 Hz sampling frequency (i.e., a PRI of 4 ms) would provide excellent results for heart rate variability (HRV) analysis [53], while an SNR of 20 dB is sufficient to obtain a good detection [54]. A SISO FMCW radar using a mechanical antenna rotation system was proposed to perform 2-D localization [55]. However, a mechanical scanning system might not be preferable in some applications, being bulky, expensive and typically slower than an electronic solution. The same considerations on the trade-off between radiated power and PRI apply also for the mechanical beam-steering SISO radar because, also in this case, multiple waveforms should be transmitted to cover the whole environment. The main contributions of this article are as follows.

1) A SISO UWB FMCW radar sensor integrating two rampart line antennas, one for the transmission and one for the reception, is presented for concurrent 2-D localization (range and azimuth) and vital signs motioning of multiple subjects. This contrasts current state-of-the-art SISO approaches. Besides requiring only two antennas and involving lower power consumption, complexity, and amount of data to be transferred/processed, another advantage over a MIMO system is in the modality the angular information in retrieved. In fact, with a MIMO radar, the information along one specific direction is reconstructed combining properly signals collected by low gain omnidirectional radiating sources. With the proposed system, instead, only one direction a time is illuminated by the electromagnetic radiation with a high gain beam. This allows minimizing the influence of other targets and/or static reflectors present in other directions, namely the multi-paths. This architecture has advantages also over standard beam-steering radars because, as it will be detailed in the next Sections, it requires only transmitting two waveforms to cover the whole environment. This allows also relaxing the system design and the PRI. Moreover, this radar satisfies all the worldwide indoor UWB spectral mask requirements [10].
2) A data processing algorithm is described to perform concurrent 2-D localization and vital signs monitoring on multiple subjects and to get rid of static reflectors (i.e., clutter, objects, etc.).
3) *In vivo* demonstration of the proposed radar sensor by accurately capturing individual heart rates, respiration rates, and 2-D locations of paired volunteers in a real-world office setting.

The idea of using frequency-scanning antennas in combination with a radar system was presented also in [55]–[59]. Those works focus on surveillance purposes and on profile reconstruction of indoor scenarios (e.g., a kitchen entrance area) or metallic objects (e.g., detection of concealed weapons and buried objects). Moreover, they are mainly based on simulations, showing limited results based on proof-of-concept measurements. To our best knowledge, a SISO FMCW radar sensor integrating two rampart line antennas was never demonstrated for concurrent localization and vital signs monitoring of multiple human subjects. Due to nature of

This article has been accepted for publication in a future issue of this journal, but has not been fully edited. Content may change prior to final publication. Citation information: DOI 10.1109/JIOT.2021.3051580, IEEE Internet of Things Journal

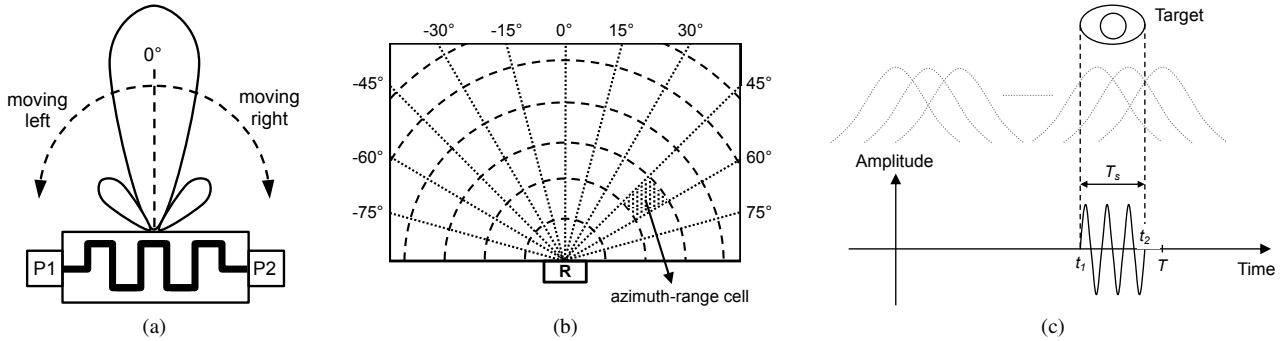

(a) (b) (c)

Fig. 1. Operational principle of the rampart line antenna. (a) Scanning principle. (b) Graphical illustration of the division of an environment in azimuth-range cells. (c) Baseband signal resulting from the proposed system. Only few beams invest the target. In the figure, the dotted lines depict the simplified gain profile of the scanning beam over time.

the physiological parameters, involving very subtle rhythmic changes in the reflected radar signature, the proposed approach requires different data processing techniques than the ones reported in [56]–[60].

The remainder of this article is organized as follows. In Section II, the operation principle of the rampart antenna together with an FMCW radar sensor is explained. In Section III, the radar system architecture is presented. In Section IV, the data processing algorithm is detailed. Experimental results from human volunteers are shown in Section VI.

II. Operational Principle

A rampart line antenna is a microstrip frequency scanning radiator, realised with a cracked microstrip line (see Fig. 1a). It acts as a 1-D array of radiators, whose elementary sources are represented by the microstrip bends and the phase shifts between two consecutive radiators are defined by the interconnecting lines whose electrical lengths are frequency dependent. The antenna is designed to operate in the same frequency range of the transmitted FMCW signal (called *chirp*). The scanning principle can be easily explained with the help of Fig. 1a. The direction of main beam can be modified both by changing the feeding port, as the antenna is a two-port travelling wave device (P1 and P2), and by increasing the instantaneous transmitted frequency. During the normal operation, one port is connected to the microwave source while the other to a 50 Ω load. More precisely, when the antenna is fed from P1 and a matched load is connected to P2, the main antenna beam points at 0° at the lowest frequency of the *chirp* and its direction rotates to the right (i.e., clockwise) while increasing the frequency. Since the antenna is symmetric, when the load and the feed are inverted, the main beam points again at 0° at the lowest frequency of the *chirp* but this time its orientation rotates to the left (i.e., counter-clockwise) while increasing the frequency. As it will be detailed in Section IV, this operation corresponds to ideally divide an environment in azimuth-range cells whose lengths depend on the radar range resolution (i.e., range bins size) and the widths on the angular resolution defined by the antenna beam and by the data processing algorithm (Fig. 1b). Therefore, each azimuth-range cell is characterized by a unique absolute distance / angular sector combination.

For a generic FMCW radar, the baseband signal $a(t)$ resulting from a motionless target at a distance d away from the antenna can be expressed as

$$a(t) = A \sin\left[2\pi\left(\frac{B}{T}\frac{2d}{c}t + f_0\frac{2d}{c}\right)\right], \tag{1}$$

where A is the voltage amplitude, c is the speed of light in free space, while f_0, T, and B are respectively the initial frequency, the duration, and the bandwidth of the *chirp*. Since the antenna beam has a certain directivity and it is continuously scanning, each target is illuminated with sufficient power by the electromagnetic radiation only during an interval T_s = t_2 - t_1 smaller than T (Fig. 1c), therefore the resulting baseband signal $s(t)$ can be modelled as

$$s(t) = \begin{cases} a(t) & \text{when } t_1 \le t \le t_2 \\ 0 & \text{elsewhere} \end{cases}. \tag{2}$$

III. Radar Sensor

The block diagram and the photo of the radar sensor are shown in Fig. 2. It consists of a radar block and of two identical rampart line antennas.

A. Radar Architecture

The core element is represented by the imec's 8 GHz UWB radar IC (integrated circuit), which is based on a digital linear discrete FMCW (LD-FMCW) architecture. An LD-FMCW radar is essentially a linear FMCW with the benefit of the digital implementation [37]. The chip, fabricated in 40 nm CMOS, integrates the LD-FMCW source, a mixer, a low-noise amplifier (LNA), an active band pass filter (BPF), and a 9-bit analog-to-digital converter (ADC). The output of the LD-FMCW source is divided in two branches which are connected respectively to the external Mini-Circuits ZX60-06203LN+ power amplifier (PA) and internally to the mixer's local oscillator port (Fig. 2a). Details on the chip are reported in [38], [39].

In order to alternatively feed the antennas' ports to perform the beam scanning, two SP8T EV1HMC321ALP4E boards have been used. More precisely, to scan the beam from 0° to the right, the SW1 and SW3 switches connect the P1 ports respectively to the PA and the LNA while the SW2 and SW4

This article has been accepted for publication in a future issue of this journal, but has not been fully edited. Content may change prior to final publication. Citation information: DOI 10.1109/JIOT.2021.3051580, IEEE Internet of Things Journal

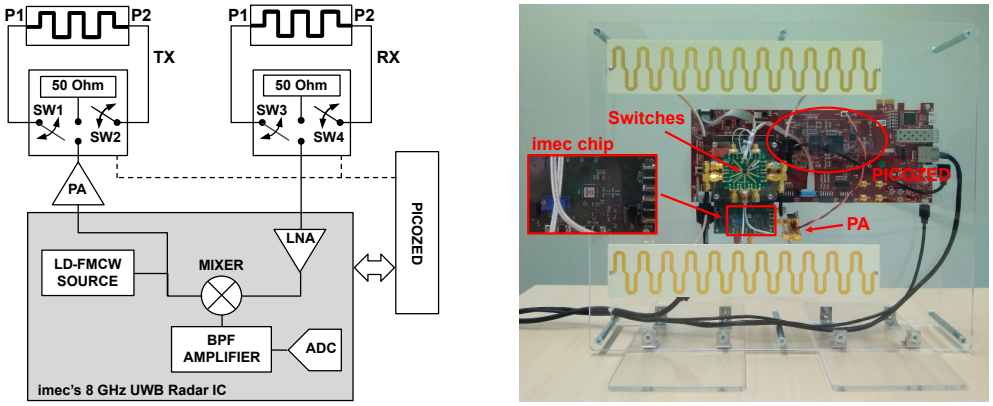

(a) (b)

Fig. 2. Radar sensor. (a) Block diagram. (b) Set-up photo.

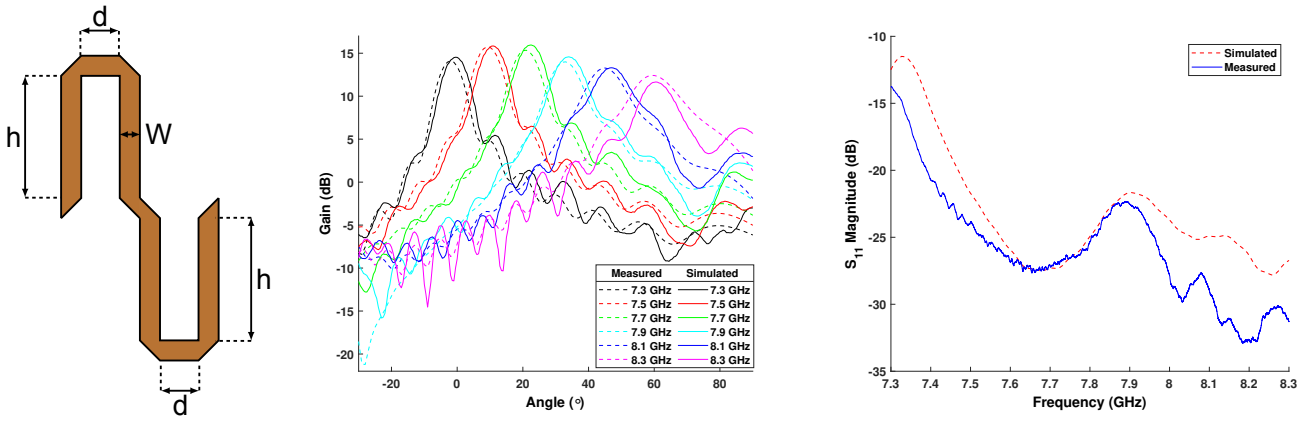

(a) (b) (c)

Fig. 3. (a) Geometry of the periodic structure of the designed antenna. Simulated and measured (b) radiation patterns and (c) reflection coefficient magnitude.

switches connect the P2 ports to 50 Ω. On the other hand, to scan the beam from 0° to the left, the SW1 and SW3 switches connect the P1 ports to 50 Ω while the SW2 and SW4 switches connect the P2 ports respectively to the PA and the LNA. The imec's 8 GHz UWB radar chip is mounted on a PCB which is connected through a PicoZed Carrier Card V2 to the PicoZed7015. The latter configures the chip, reads the data from the ADC, controls the EV1HMC321ALP4E boards, and sends the data to the laptop.

The radar transmits *chirps* of duration T = 40.96 µs, initial frequency f_0 = 7.3 GHz and total bandwidth B = 1 GHz, which results in a range resolution of 15 cm. During this interval, considering the ADC sampling rate of 12.5 MHz, 512 samples are obtained in the *fast time*. The *chirps* are transmitted with a PRI of 1.3 ms where a *chirp* is used to scan the beam to the left while the subsequent to the right. This involves an effective sampling time t_s in *slow time* of 2.6 ms. With this waveform configuration and with a power of −6 dBm feeding the PA, the chip consumes a record average power of only 680 µW [38], [39]. Considering the losses of the EV1HMC321ALP4E boards and the cables, and the maximum gain of the transmitting antenna, an external PA is used to set the effective radiated peak power to 0 dBm. The waveform configuration together with the transmitting power allows satisfying the limits of all the worldwide UWB indoor radio regulations in terms of both power spectral density (−41.3 dBm/MHz) and peak power (0 dBm/50 MHz) [10]. Details on the FMCW working principle and on the radar terms (e.g., *fast-slow time*, ...) can be found in [40], [55].

B. Rampart Line Antenna

For the transmitting and receiving antennas two identical rampart line antennas [61]–[64] have been designed to operate in the 7.3 GHz-8.3 GHz frequency range. This radiator topology is a frequency scanning microstrip antenna that has been preferred over other solutions available in the literature (i.e. slotted waveguide) due to to its compactness, low cost and easiness of realization. Furthermore, being a travelling wave antenna, this radiator is intrinsically wideband, representing an optimal solution for the proposed radar system, whose fractional bandwidth is of about 13%.

A rampart line antenna appears as a cracked microstrip line that operates as a 1-D array of radiators. The main source of radiation is represented by the magnetic currents on the corner edges. The interconnecting microstrip lines (vertical and horizontal lines in Fig. 3a) act mainly as phase shifters between two consecutive bends. Since the shift introduced by the lines is frequency dependent, the main beam direction varies with frequency. The number of corners, representing the radiation sources, controls both the antenna gain and the

main lobe angular width (beamwidth). The proposed antenna consists of a series of 11 equal structures (Fig. 2b), for a total size of 27.3 × 5.3 cm^2, and it was designed on a 1.524 mm thick Rogers RO4350B substrate. A narrow beamwidth is fundamental to guarantee the angular separation necessary to distinguish multiple targets. The number of periods was chosen to maximize the gain and minimize the power dissipated in the matched load. A further increase in the number of periods would only result in the reduction of the antenna performance, due to the higher losses in the dielectric and in the metallic parts, without any further reduction in the antenna beamwidth. With the proposed design, the antenna efficiency increases from 0.71 to 0.83 within the 7.3-8.3 GHz range.

The antenna geometrical parameters are: d = 5 mm, W = 3.5 mm, and h = 16.5 mm (Fig. 3a). With those values, the antenna scans an angular range of about 60° per direction of rotation, with a gain varying inside the 12.4 dB-15.8 dB range and with a 3 dB beamwidth which varies from 8.5° at 7.3 GHz to 17.7° at 8.3 GHz (Fig. 3b). Measurement results of both the Cartesian gain-angle plots (Fig. 3b) and the reflection coefficient S_{11} (Fig. 3c) are in really good agreement with simulations.

IV. Data Processing

A. Azimuth-range cells definition

The baseband signals resulting from the *chirps* are transferred real-time to a laptop and read using a Matlab script. The data is arranged in two matrices, namely the *left matrix* M_L and the *right matrix* M_R, depending on whether it contains information from the left sectors or from the right sectors. Each matrix consists of $N_c = 512$ columns, containing the ADC samples acquired in the *fast time* each $t_f = 80$ ns, and of a number of rows N_r which depends both on the sampling time in *slow time* t_s and on the length of the monitoring interval. Since the pointing direction of the antenna varies with the frequency, each target is illuminated by the electromagnetic radiation for a time T_s smaller than the *chirp* duration T (Fig. 1c). Consequently, the information of a single target (range, angle, and vital signs) is encoded only in a sub-matrix m_{sub} of one of the two matrices (M_L and M_R), namely only in some of the N_c columns. This means that the information of multiple targets at different angular orientations are encoded in different sub-matrices. Therefore, in order to perform angular separation, the two matrices have to be divided in $N_r \times N_w$ sub-matrices, where N_w is the number of columns (or samples in *fast time*) expected being influenced by a subject while the beam is scanned. Moreover, in order to have a fine angular resolution, an overlap of s_w columns should be considered. For the targeted application, N_w and s_w have been opportunely chosen considering the size of a human individual and of a typical room setting. The designed rampart line antenna can scan a total of 60° per *chirp*, either from 0° to −60° rotating to the left or from 0° to 60° rotating to the right, resulting in 512 digitized baseband signal samples. Therefore, desiring a size of 15° per angular sector, each sub-matrix should contain $N_w = 128$ columns. The overlap among sub-matrices s_w has been chosen equal to 64 columns, which corresponds to an angular step of 7.5°. This results in dividing the room environment in 14 equal-spaced angular sectors, namely from 0° to ±15°, from ±7.5° to ±22.5°, from ±15° to ±30°, from ±22.5° to ±37.5°, from ±30° to ±45°, from ±37.5° to ±52.5°, and from ±45° to ±60°. A target that is detected in one of those sectors would be oriented in the middle of it, namely respectively at ±7.5°, ±15°, ±22.5°, ±30°, ±37.5°, ±45°, and ±52.5°.

B. Signal analysis

From (2) and considering normally breathing subjects, the digitized data in each sub-matrix can be fairly expressed as

$$m_{sub}(n,m) = \sum_i A_i(mt_s) \cdot \sin\left[2\pi\left(\frac{B}{T}\frac{2d_i(mt_s)}{c}nt_f + f_0\frac{2d_i(mt_s)}{c}\right)\right], \quad (3)$$

where i is the index corresponding to the i-th target/object, n = 0, ..., N_w-1 and m = 0, ..., N_r-1 are respectively the *fast time* and *slow time* indexes, and with

$$d_i(mt_s) = \begin{cases} d_{0,i} + x_i(mt_s) & \text{for human target} \\ d_{0,i} & \text{for clutter/object} \end{cases}, \quad (4)$$

where d_0 indicate the nominal target's absolute distance (this description considers seated/lying down subjects) and $x(mt_s)$ is the vital signs information (i.e., the chest-wall motion caused by the heartbeat and respiration). The latter can be expressed as:

$$x(mt_s) = x_r(mt_s) + x_h(mt_s) = \\ = X_r sin(2\pi f_r mt_s) + X_h sin(2\pi f_h mt_s), \quad (5)$$

where $x_r(mt_s)$ and $x_h(mt_s)$, approximated as periodic functions, indicate respectively the mechanical displacements produced by the respiration and the heart (i.e., cardiopulmonary activity) on the chest/wall surface, X_r and X_h have typical amplitudes respectively around 4 mm-12 mm and 0.1 mm-0.5 mm, while f_r and f_h are the vital signs frequencies which, depending on the subject and on the health condition, are within the 0.1 Hz-3 Hz range [4]. Equation (3) is valid for *chirp* duration T sufficiently shorter than the periods of the vital signs motions (*stationary target assumption*) [32]. If so, the target is essentially motionless during T and it can be assumed to be frozen at $d_0 + x(mt_s)$. If that condition is not ensured, there will be range / Doppler ambiguities and (3) is no longer valid. In this work, $T = 40.96$ µs is almost four orders shorter than the shortest heartbeat period, which in extreme conditions is about 0.33 s (corresponding to about 3 Hz). Therefore, the assumption on stationary target results valid.

For each sub-matrix, each row (of 128 samples) has been multiplied by a Hann window $w(n)$ and then padded with $N - N_w = 384$ zeros to have the same length of a baseband signal produced by the proposed radar system but integrating a non-scanning antenna (i.e., a classic FMCW). The first step to retrieve the target information is to apply the fast Fourier transform (FFT) to each sub-matrix per rows (i.e., in *fast time*),

generating 14 new matrices of $N_r \times 512$ complex samples, each can be expressed as

$$M_{sub}(k,m) = \mathscr{F}\{ZeroPad\,[m(n,m)\cdot w(n)]\} = \sum_i \frac{A_i(mt_s)}{2} W\left(\frac{k}{K} - \frac{\overline{B}}{\overline{T}}\frac{2d_i(mt_s)}{c}t_f\right) e^{j\left(\frac{4\pi f_0 d_i(mt_s)}{c} - \frac{\pi}{2}\right)} + \sum_i \frac{A_i(mt_s)}{2} W\left(\frac{k}{K} + \frac{\overline{B}}{\overline{T}}\frac{2d_i(mt_s)}{c}t_f\right) e^{j\left(\frac{\pi}{2} - \frac{4\pi f_0 d_i(mt_s)}{c}\right)}, \quad (6)$$

with

$$W(k) = \frac{1}{2}D_N(k) + \frac{1}{4}D_N(k+1) + \frac{1}{4}D_N(k-1), \quad (7)$$

where $\mathscr{F}$ is the FFT operator, $w(n)$ and $W(k)$ are a Fourier pair, k = 0, ..., K-1 being the frequency bin index, $K = N_c$, D_N is the Dirichlet kernel, and the variables $\overline{B}$ and $\overline{T}$ are respectively the total bandwidth and the *chirp* duration taking into account the zero-padding operation. The frequency bins are then converted in range bins considering only positive frequencies and remembering that the frequency is proportional to the range through $2\overline{B}/(c\overline{T})$ [55]. It should be clarified that the zero-padding operation does not improve the range resolution but improves the range accuracy, which is limited by the radar noise. Therefore, if in the same angular sector there is only one subject or multiple targets which are separated in range by at least the reduced range resolution, the target(s) will be located at the range bin(s) as in the case of a classic FMCW. Obviously, if multiple targets are closer in range than reduced range resolution, even busting the zero-padding till the limit set by the radar noise, the system will never be able to resolve them. The FFT allows also reducing the amount of data. In fact, assuming that the environment is 6 m long, only the first 41 columns need to be considered, namely the first 41 range bins spaced of 15 cm.

C. 2-D localization and vital signs monitoring

In order to distinguish human beings from static clutter/objects and to perform 2-D localization, the standard deviation (std) operation is applied to the complex samples of the 14 M_{sub} matrices per column, namely to (6) in *slow time*. The idea is that the physiological movements involve a larger std than static objects [55]. For each subject, the maximum std value corresponds to the range bin nearest to $d_i(mt_s)$. Since $x(mt_s)$ is several order smaller than radar range resolution (which is limited by B), the subject's absolute distance is determined only by d_0 which for seated/lying down target is constant in *slow time*. The std operation results in 14 vectors of 41 real value elements. The 2-D localization can be obtained by arranging the std results into a 41 (i.e., range bins) $\times$ 14 (i.e, angular sectors) matrix. The indexes of elements of this matrix corresponding to the local maxima indicate the targets' locations. From this information is possible to determine the azimuth-range cells, namely the range bin / angular sector combinations, where the subjects are.

Due to the limited resolution of the FFT and since $x(mt_s)$ is very small, the frequency information retrieved from (6) cannot be used to monitor the vital signs. The latter operation however can be performed looking at the phase information in *slow time* (i.e., Doppler signal) as the received *chirps* are significantly phase modulated by the chest motion (Doppler effect) [40], [55]. The vital signs information is obtained after performing 2-D localization and reading the complex samples in *slow time* from the azimuth-range cell(s) where the subject(s) is(are) localized. The next step is to extract the phase information from the complex samples. However, the stationary reflectors (i.e., clutter, objects, static body parts) present in the azimuth-range cells cause a distortion of the Doppler signal [23], [24], which can jeopardize the vital signs extraction. To tackle this issue, and hence to isolate only the contribution of the cardiopulmonary activity, a phase optimization procedure is used. The complex samples from each subject are arranged in a $N_r \times 2$ matrix $\mathbf{M}$ defined as

$$\mathbf{M} = [\mathrm{real}\,(\mathbf{v})\ \ \mathrm{imag}\,(\mathbf{v})]\,, \quad (8)$$

where $\mathbf{v}$ is a vector containing the complex samples after mean removal. Then, the covariance matrix $\mathbf{C}$ of $\mathbf{M}$ is determined from which its eigenvectors are calculated. The final step is to determine the matrix $\mathbf{S}$ containing the principal components:

$$\mathbf{S} = \mathbf{E}^{\mathrm{T}}\mathbf{M}^{\mathrm{T}}, \quad (9)$$

where $\mathbf{E}$ is a matrix whose columns are the eigenvectors of $\mathbf{C}$ and the superscript T indicates the transpose operator. The first principal component is the optimized Doppler signal s_i containing only the variable information:

$$s_i(m) \approx \frac{4\pi f_0}{c} x_i(mt_s). \quad (10)$$

The data processing description might mislead the reader that the proposed system has an issue in detecting a target at 0°. In fact, it should be approximated either at 7.5° or at -7.5°, giving an angular error equal to 7.5° while in all the other sectors the maximum error would be of 3.75° (i.e., half of the angular step). However, as it will be demonstrated in the experimental results section, this can be easily solved looking separately at the local maxima from the 0° to ±15° sectors. In fact, a target a 0° would produce two mirrored local maxima, namely at the same absolute distance but at opposite angular orientations (±7.5°). The same vital signs information is obtained from the Doppler signals extracted from those two local maxima, by which it is possible to state that there is only one subject at 0°.

V. Simulations

Simulations have been performed to prove theoretically the proposed system and data processing algorithm. Four different scenarios have been considered where there are always present two persons. The parameters of Subject 1 are: X_r = 4 mm, X_h = 0.2 mm, f_r = 0.2 Hz and f_h = 1 Hz; while for Subject 2 are: X_r = 5 mm, X_h = 0.4 mm, f_r = 0.3 Hz and f_h = 1.2 Hz. The simulations also took into account the parameters (i.e., receiver's noise figure, transmitter's phase noise profile, ...) of the imec's 8 GHz UWB radar IC [38], [39].

This article has been accepted for publication in a future issue of this journal, but has not been fully edited. Content may change prior to final publication. Citation information: DOI 10.1109/JIOT.2021.3051580, IEEE Internet of Things Journal

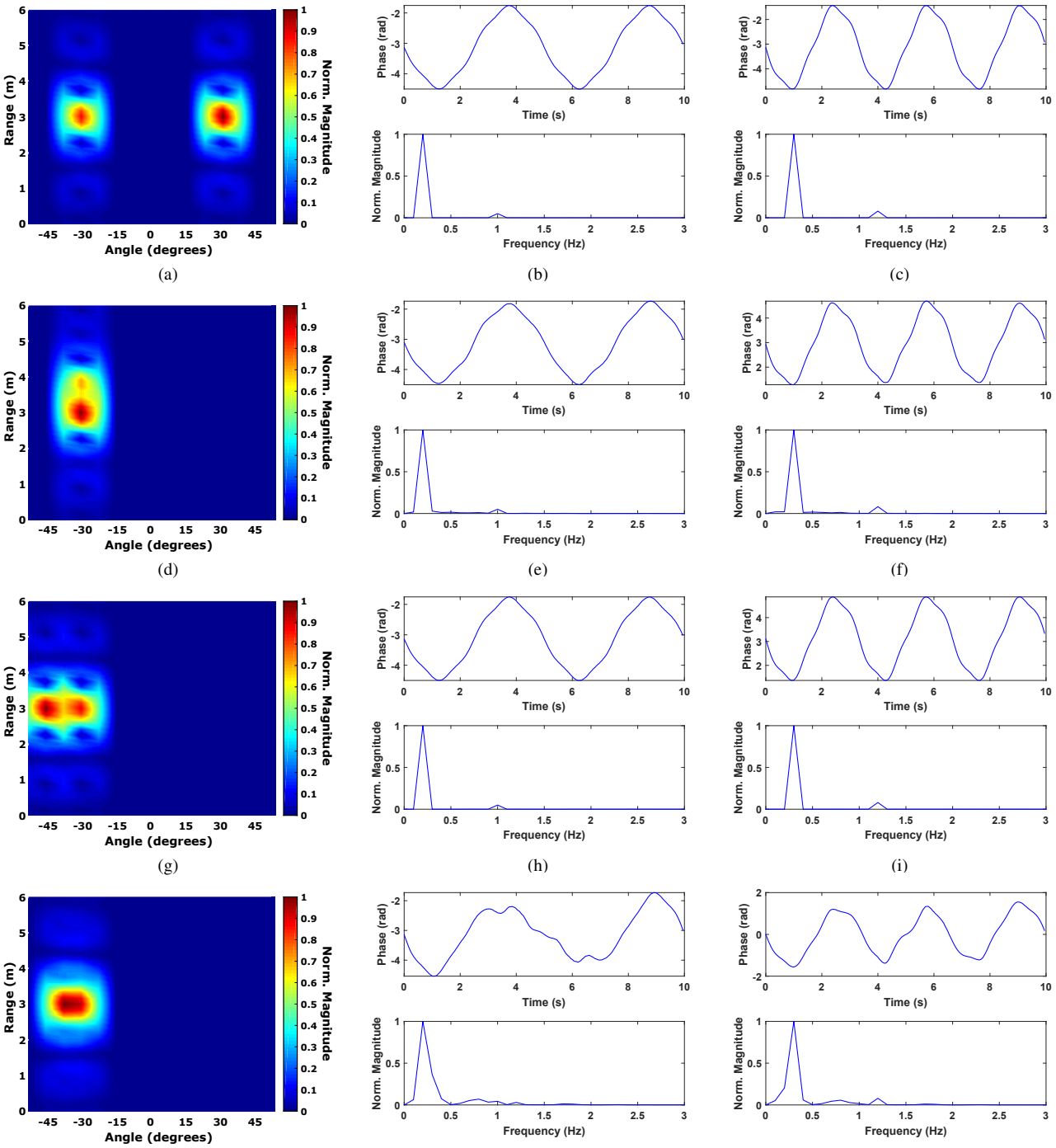

Fig. 4. Simulation results. (a)-(c) Subject 1 at 3 m and −30° and Subject 2 at 3 m and 30°. (a) 2-D localization. (b) Extracted Doppler signal from Subject 1 and resulting spectrum. (c) Extracted Doppler signal from Subject 2 and resulting spectrum. (d)-(f) Subject 1 at 3 m and −30° and Subject 2 at 3.8 m and −30°. (d) 2-D localization. (e) Extracted Doppler signal from Subject 1 and resulting spectrum. (f) Extracted Doppler signal from Subject 2 and resulting spectrum. (g)-(i) Subject 1 at 3 m and −30° and Subject 2 at 3 m and −45°. (g) 2-D localization. (h) Extracted Doppler signal from Subject 1 and resulting spectrum. (i) Extracted Doppler signal from Subject 2 and resulting spectrum. (j)-(l) Subject 1 at 3 m and −30° and Subject 2 at 3 m and −37.5°. (j) 2-D localization. (k) Extracted Doppler signal from Subject 1 and resulting spectrum. (l) Extracted Doppler signal from Subject 2 and resulting spectrum. In the spectra, the highest and the smallest peaks correspond respectively to the respiration and heartbeat fundamentals.

Figures 4a-c show the simulation results with two subjects in the same range bin at 3 m but at opposite angular orientations at ±30°. The two targets have been correctly resolved and the vital signs properly extracted.

Figures 4d-f regard two targets in the same angular sector at -30°. Subject 1 was at 3 m while Subject 2 at 3.8 m. Since in this work, and hence also in these simulations, the submatrices of N_w = 128 columns are obtained from the M_L and

This article has been accepted for publication in a future issue of this journal, but has not been fully edited. Content may change prior to final publication. Citation information: DOI 10.1109/JIOT.2021.3051580, IEEE Internet of Things Journal

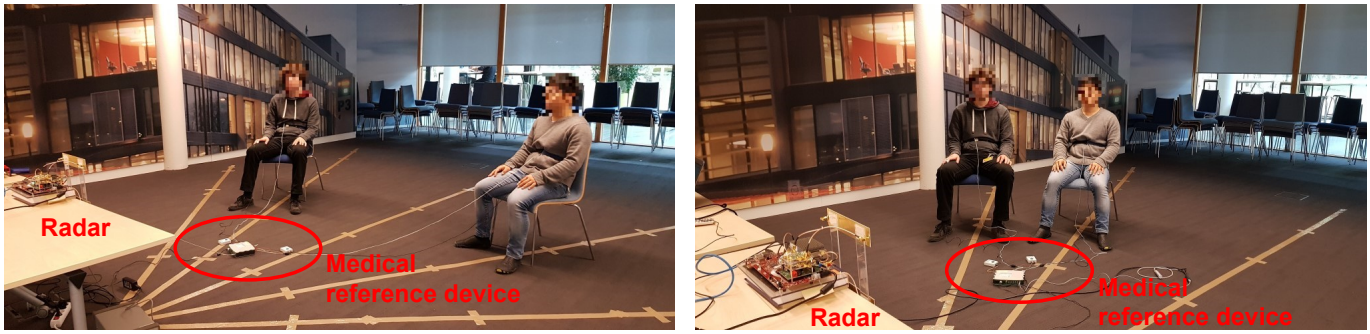

(a) (b)

Fig. 5. Experimental environment and set-up. (a) Subject 1 was sat on a chair in a left sector while Subject 2 in a right sector. (b) Subject 1 and Subject 2 close each other in two adjacent angular sectors.

M_R matrices of $N_c = 512$ columns, the proposed system has a total bandwidth 4 times smaller than the one that would have a classic FMCW. This involves a range resolution of 60 cm. Since the two targets are separated in range by a distance which is larger than the range resolution, they have been properly monitored. It can be noticed from the 2-D map that Subject 1 presents the strongest contribution although his/her simulated cardiopulmonary activity involves smaller motions than the ones of Subject 2. This is because the simulation includes also the effect of the path-loss. Nevertheless, the Doppler signals are properly extracted, showing in the Doppler profiles the correct difference between the amplitudes of the physiological motions of the two targets. This simulation demonstrates the concept stated in Subsection IV-B regarding the improvement of the range accuracy due to the zero-padding. Subject 2 was in fact located at 3.75 m which is a integer multiple of 15 cm (as for a classic FMCW). Without zero-padding, the target would have been located at 3.6 m which is an integer multiple of 60 cm (i.e., the reduced range resolution). This simulation considers a scenario where the subjects are one behind the other. During real experiments, this is a very challenging situation for monitoring. In fact, the closest person will obstruct the transmitted waveform to reach the farther target, therefore its reflection will be strongly attenuated to not fall within the receiver's dynamic range. Moreover, the multipath generated by Subject 1 will inevitably interact with the direct reflection of Subject 2, generating non-linear combinations of the Doppler signals and therefore jeopardizing the localization and the vital signs extraction.

Figures 4g-i show an example with the two subjects at the same absolute distance of 3 m but separated by one angular sector (in this work is 15°). More precisely, Subject 1 is at -30° and Subject 2 at -45°. In this case, the subjects were correctly monitored. However, this represents a limit situation. If the two targets, at the same absolute distance, get closer in angular dimension by less than one angular sector (i.e., less than 15°), they could not be correctly monitored. This is demonstrated in Figs. 4j-l, representing a scenario with Subject 1 and 2 both at 3 m but at -30° and -37.5°, respectively. From Fig. 4j it is possible to notice two significant peaks, one at 3 m and -30° and the other at 3 m and -37.5°. However, they are not both local maxima. The only local maximum is at 3 m and -37.5°. This is because Subject 2 has a stronger simulated cardiopulmonary activity. The same outcome is experienced while extracting the vital signs (Fig. 4k-l). In fact, although there is some small unwanted harmonics, Subject 2 have been properly monitored while for Subject 1 only the respiration rate was correctly retrieved (the respiration involves a stronger motion than the heartbeat). Since the two target are closer than one angular sector, the non-linear interaction of their Doppler signals becomes no longer negligible.

VI. Experimental Results

Experimental evaluations have been conducted monitoring two subjects at the same time who were invited to breath normally (Fig. 5). The sensor was put on a desk at about 1 m of height. The g.USBamp device (CE certified and FDA cleared medical device, safety class: II, conformity class: IIa, type of applied part: CF), integrating two photoplethysmogram (PPG) finger sensors and a two respiration belts, was used as gold standard reference for heartbeat and respiration. Traces were marked with tape on the floor to indicate the absolute distances and the angular sectors.

A. 2-D localization and vital signs monitoring

Fig. 6 shows the results of a measurement of 30 seconds with Subject 1 at 2 m and −30° and Subject 2 at 2 m and 30°. Fig. 6a shows the obtained 2-D map (range vs. angle) by which the two local maxima indicate correctly the position of the two volunteers. The resulting vital signs signals and the corresponding spectra are shown in Figs. 6b,c in which it is possible to observe perfect matches with the references (PPGs and belts). The same considerations can be also made for the experiment shown in Fig. 7, where Subject 1 was at 3 m and −45° and Subject 2 at 3 m and 45°, and for the experiment shown in Fig. 8, where Subject 1 was at 4 m and −30° and Subject 2 at 4 m and 30°. It can be noticed that in some measurements, it was possible to retrieve not only the first harmonic of the heartbeat but also the second one. This is fundamental for applications where it is necessary to determine accurate HRV, namely the variance in time between the beats. This time domain information is very hard to retrieve using only the heartbeat fundamental [53].

In the aforementioned measurements, the two subjects were placed at the same range bin but at opposite angular sectors.

This article has been accepted for publication in a future issue of this journal, but has not been fully edited. Content may change prior to final publication. Citation information: DOI 10.1109/JIOT.2021.3051580, IEEE Internet of Things Journal

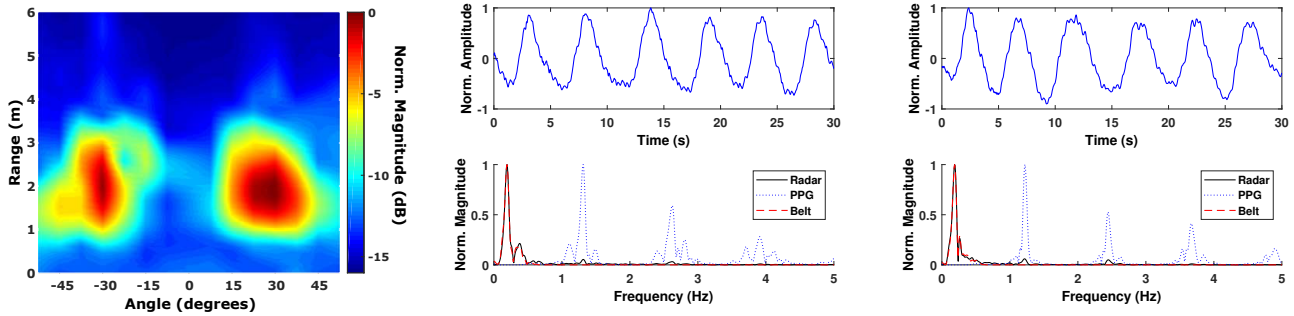

(a) (b) (c)

Fig. 6. Experimental results with Subject 1 at 2 m and −30° and Subject 2 at 2 m and 30°. (a) 2-D localization. (b) Extracted Doppler signal from Subject 1 and resulting spectrum. (c) Extracted Doppler signal from Subject 2 and resulting spectrum.

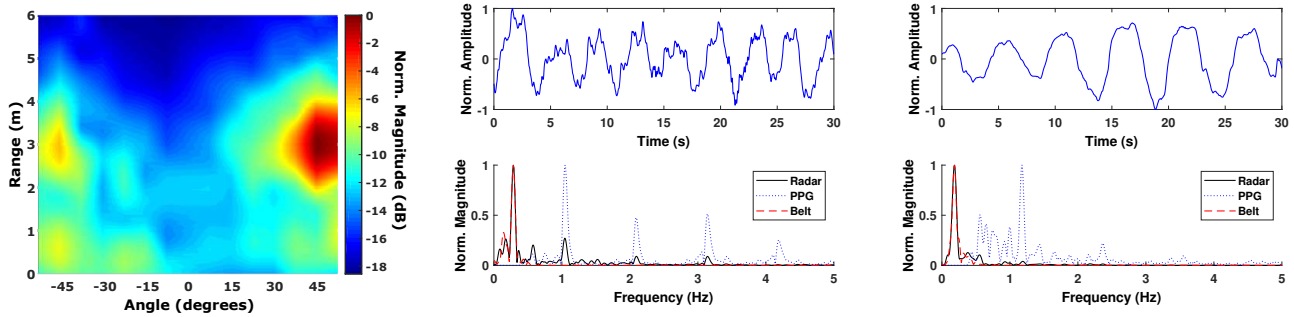

(a) (b) (c)

Fig. 7. Experimental results with Subject 1 at 3 m and −45° and Subject 2 at 3 m and 45°. (a) 2-D localization. (b) Extracted Doppler signal from Subject 1 and resulting spectrum. (c) Extracted Doppler signal from Subject 2 and resulting spectrum.

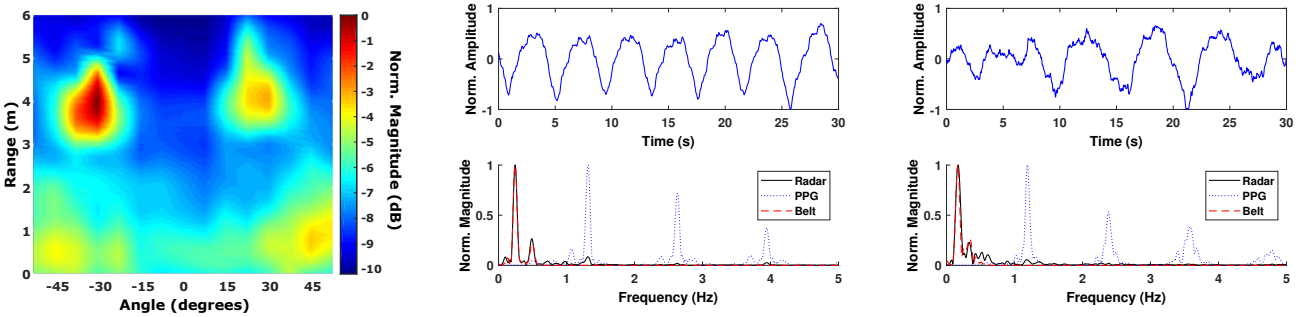

(a) (b) (c)

Fig. 8. Experimental results with Subject 1 at 4 m and −30° and Subject 2 at 4 m and 30°. (a) 2-D localization. (b) Extracted Doppler signal from Subject 1 and resulting spectrum. (c) Extracted Doppler signal from Subject 2 and resulting spectrum.

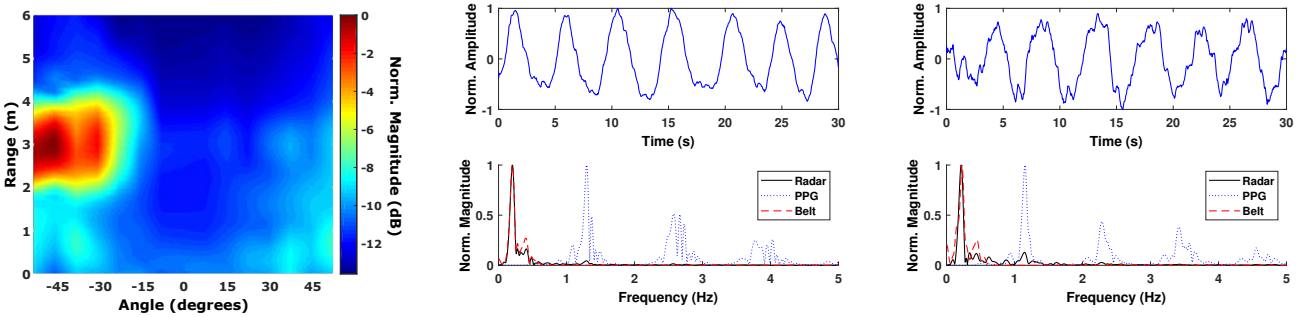

(a) (b) (c)

Fig. 9. Experimental results with Subject 1 at 3 m and −45° and Subject 2 at 3 m and −30°. (a) 2-D localization. (b) Extracted Doppler signal from Subject 1 and resulting spectrum. (c) Extracted Doppler signal from Subject 2 and resulting spectrum.

This article has been accepted for publication in a future issue of this journal, but has not been fully edited. Content may change prior to final publication. Citation information: DOI 10.1109/JIOT.2021.3051580, IEEE Internet of Things Journal

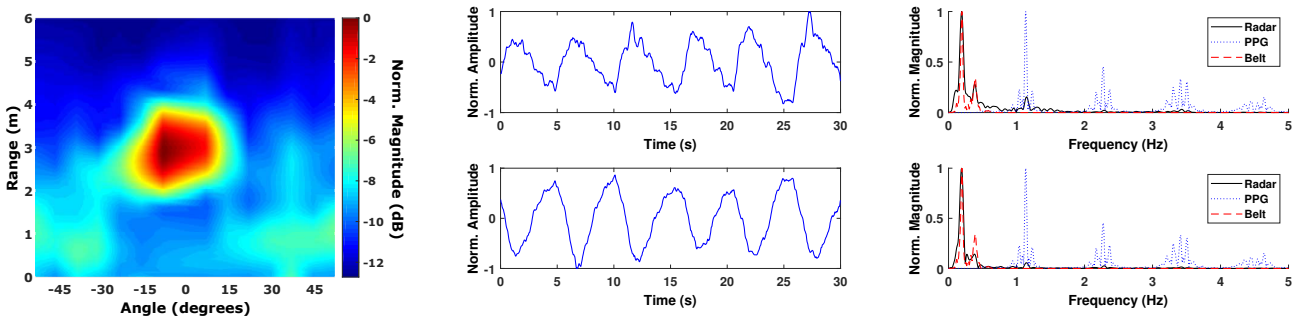

(a) (b) (c)

Fig. 10. Experimental results with a subject at 3 m and 0°. (a) 2-D localization. (b) Doppler signals and (c) resulting spectra obtained from the 3 m / −7.5° (top plots) and 3 m / 7.5° (bottom plots) azimuth-range cells.

TABLE I
PERFORMANCE FOR DIFFERENT ABSOLUTE DISTANCES AND ORIENTATIONS

	Scenarios							
	2m 0°	**3m 0°**	**4m 0°**	**2m ±30°**	**2m ±45°**	**3m ±30°**	**3m ±45°**	**4m ±30°**
MAE RR Subject 1 (BPM)	0.048	0.208	0.243	0.071	0.232	0.223	0.209	0.747
MAE HR Subject 1 (BPM)	0.291	0.330	1.428	0.329	2.359	1.341	2.645	2.608
MAE RR Subject 2 (BPM)	–	–	–	0.049	0.140	0.224	0.194	0.041
MAE HR Subject 2 (BPM)	–	–	–	0.374	0.146	1.404	2.601	0.178

Those tests proved that the proposed radar sensor can resolve targets in the same range bins. However, the volunteers were separated each other by few meters. Fig. 9 shows an experiment where the subjects were at the same range bin but separated by one angular sector (i.e., 15°). More precisely, Subject 1 was at 3 m and −45° and Subject 2 at 3 m and −30° (Fig. 9b). Also in this case, the radar sensor was able to properly locate the two volunteers showing high capability is resolving close targets (Fig. 9a). This is also confirmed by the extracted vital signs signals and by the corresponding spectra which perfectly match the references (Figs. 9b,c).

Finally, Fig. 10 shows an example of a subject at 3 m and 0°. Looking at the 2-D map in Fig. 10a and considering separately the left and right sectors, there are two local maxima corresponding to the −7.5° / 3 m and 7.5° / 3 m azimuth-range cells. From the Doppler signals extracted from those two positions (Fig. 10b), which present obviously similar trends but different initial phases, the same vital signs rates are obtained which are also in agreement with the references (Fig. 10c). Therefore, it is possible to conclude that there is only one target at 3 m and 0°.

B. Impact of distance and orientation

In order to evaluate the effects of the distance and orientation on the system, 16 experiments have been performed on 5 subjects, 4 males and 1 female, differing in height (160-190 cm), in weight, and in age (24 - 35 years), invited to randomly chose a seat and to breathe normally. Eight different scenarios have been selected, namely a single subject at 2m and 0°, at 3m and 0°, and at 4m and 0°, and two subjects (i.e., Subject 1 and Subject 2) at 2m and ±30°, at 2m and ±45°, at 3m and ±30°, at 3m and ±45°, and at 4m and ±30°. For each scenario and subject, 2 measurements of 60 seconds have been collected. The vital signs signals, extracted using the technique described in Section IV-C, have been processed using sliding windows of 20 seconds with overlaps of 19 seconds. The respiration and heartbeat signals have been retrieved from the vital signs signals using the Wavelet decomposition and the corresponding rates have been estimated using the FFT. Each signal window has been zero padded by 5-time the window's size. The extracted respirations rates and heartbeats have been compared with the values obtained using the medical reference device in order to calculate the mean absolute errors (MAEs).

The results of this study have been reported in Table I, where the MAEs are expressed in terms of BPM which stands respectively for breaths-per-minute and beats-per-minute whether it refers to respiration rate (RRs) and heart rates (HRs). This experimental validation demonstrated that the proposed system is capable of properly monitoring subjects within practical indoor room settings. The maximum reported MAE for respiration rate is 0.747 BPM (subject at 4 m and 30°) while for heartbeat is 2.645 BPM (subject at 3 m and 45°). An error less than 3 BPM while estimating the heart rate is considered clinically acceptable [65].

The proposed radar sensor has been also compared with alternative state-of-the-art approaches. The results, reported in Table II, shows that this work achieves better performance than the compared solutions. This is also due to the fact that the used method optimizes the phase extraction reducing the distortion caused by stationary reflectors (i.e., clutter, objects, static body parts). Moreover, the achieved results confirm the benefit of using sub-10 GHz radars to monitor subjects in typical room settings as the SNR degrades with the distance slower than mm-wave solutions.

TABLE II
COMPARISON OF THIS WORK WITH ALTERNATIVE STATE-OF-THE-ART APPROACHES

	This work FMCW 7.3-8.3 GHz	[29] CW 5.8 GHz	[66] SFCW 2-3 GHz	[67] FMCW 5.46-7.25 GHz	[68] FMCW 9.2-10 GHz	[69] FMCW 24 GHz	[70] Monopulse 24 GHz	[51] Wi-Fi 60 GHz	[71] Wi-Fi 60 GHz
Distance (m)	2	2	1	1	2.5	3	1	2	–
MAE RR (BPM)	0.048	0.35	0.73	0.09	–	–	1.02	0.22	0.43
MAE HR (BPM)	0.291	1.14	0.42	0.95	5.15	5	–	0.92	2.15

VII. CONCLUSION

In this work, a SISO FMCW radar integrating two rampart line antennas and a data processing algorithm were described and experimentally demonstrated for concurrent 2-D localization (range and azimuth information) and vital sign monitoring of multiple subjects. The frequency scanning nature of the transmitting and receiving antennas allows performing angular separation, contrasting standard SISO systems. Compared to alternative solutions, this architecture involves lower power consumption, smaller silicon's area, simpler design and control, and a lower amount of data to be processed. This radar can be considered a useful sensor technology for the development of future smart long-term health monitoring environments.

REFERENCES

[1] O. Boric-Lubeke and V. M. Lubecke, "Wireless house calls: using communications technology for health care and monitoring," *IEEE Microw. Mag.*, vol. 3, no. 3, pp. 43–48, Sep. 2002.

[2] D. Schreurs, and M. Mercuri, "Contactless medical sensing," in *IEEE MTT-S Int. Microw. Symp. Dig.*, May 2015, pp. 1–4.

[3] D. Schreurs, M. Mercuri, P. J. Soh, and G. Vandenbosch, "Radar-Based Health Monitoring," in *Microwave Workshop Series on RF and Wireless Technologies for Biomedical and Healthcare Applications (IMWS-BIO), 2013 IEEE MTT-S International*, Dec. 2013, pp. 1–3.

[4] C. Li, V. M. Lubecke, O. Boric-Lubecke and J. Lin, "A Review on Recent Advances in Doppler Radar Sensors for Noncontact Healthcare Monitoring," *IEEE Trans. Microw. Theory Tech.*, vol. 61, no. 5, pp. 2046–2060, May 2013.

[5] C. Li *et al.*, 'A Review on Recent Progress of Portable Short-Range Noncontact Microwave Radar Systems," *IEEE Trans. Microw. Theory Tech.*, vol. 65, no. 5, pp. 1692–1706, May 2017.

[6] J. D. Taylor, *Ultra-wideband Radar Technology*, CRC Press, 2001.

[7] Z. Peng *et al.*, "A Portable FMCW Interferometry Radar With Programmable Low-IF Architecture for Localization, ISAR Imaging, and Vital Sign Tracking," *IEEE Trans. Microw. Theory Techn.*, vol. 65, no. 4, pp. 1334–1344, Apr. 2017.

[8] Z. Peng *et al.*, "Experiment and Spectral Analysis of a Low-Power Ka-Band Heartbeat Detector Measuring From Four Sides of a Human Body," *IEEE Trans. Microw. Theory Techn.*, vol. 54, no. 12, pp. 4464–4471, Dec. 2006

[9] C. Li and J. Lin, "Optimal Carrier Frequency of Non-contact Vital Sign Detectors," in *2007 IEEE Radio and Wireless Symposium*, Apr. 2007, pp. 281–284.

[10] H. W. Pflug, J. Romme, K. Philips and H. de Groot,"Method to Estimate Impulse-Radio Ultra-Wideband Peak Power," *IEEE Trans. Microw. Theory Techn.*, vol. 59, no. 4, pp. 1174–1186, Apr. 2011.

[11] F. Wang, T. Horng, K. Peng, J. Jau, J. Li and C. Chen, "Detection of Concealed Individuals Based on Their Vital Signs by Using a See-Through-Wall Imaging System With a Self-Injection-Locked Radar," *IEEE Trans. Microw. Theory Tech.*, vol. 61, no. 1, pp. 696–704, Jan. 2013.

[12] X. Liang, J. Deng, H. Zhang, and T. A. Gulliver, "Ultra-Wideband Impulse Radar Through-Wall Detection of Vital Signs," in *Sci. Rep.*, vol. 8, no. 13367, pp. 1–21, Sep. 2018.

[13] C. Gu *et al.*, "Accurate Respiration Measurement Using DC-Coupled Continuous-Wave Radar Sensor for Motion-Adaptive Cancer Radiotherapy," *IEEE Trans. Biomed. Eng.*, vol. 59, no. 11, pp. 3117–3123, Nov. 2012.

[14] D. Buxi *et al.*, "Systolic Time Interval Estimation using Continuous Wave Radar with On-body Antennas," *IEEE J. Biomed. Health Inform.*, vol. 22, no. 1, pp. 129–139, Jan. 2018.

[15] B. Y. Su, K. C. Ho, M. J. Rantz and M. Skubic, "Doppler Radar Fall Activity Detection Using the Wavelet Transform," *IEEE Trans. Biomed. Eng.*, vol. 62, no. 3, pp. 865–875, Mar. 2015.

[16] M. Mercuri, P. Karsmakers, A. Beyer, P. Leroux, D. Schreurs, "Real-time Fall Detection and Tagless Localization using Radar Techniques," in *Proc. Wireless and Microwave Techn. Conf. (WAMICON)*, Apr. 2015, pp. 1-3.

[17] A. Yang, C. Zhang, Y. Chen, Y. Zhuansun and H. Liu, "Security and Privacy of Smart Home Systems Based on the Internet of Things and Stereo Matching Algorithms," *IEEE Internet Things J.*, vol. 7, no. 4, pp. 2521–2530, Apr. 2020.

[18] J. Kua, S. H. Nguyen, G. Armitage and P. Branch, "Using Active Queue Management to Assist IoT Application Flows in Home Broadband Networks," *IEEE Internet Things J.*, vol. 4, no. 5, pp. 1399–1407, Oct. 2017.

[19] E. Anthi, L. Williams, M. Słowińska, G. Theodorakopoulos and P. Burnap, "A Supervised Intrusion Detection System for Smart Home IoT Devices," *IEEE Internet Things J.*, vol. 6, no. 5, pp. 9042–9053, Oct. 2019.

[20] P. J. Soh, G. A. E. Vandenbosch, M. Mercuri and D. M. M. Schreurs, "Wearable Wireless Health Monitoring: Current Developments, Challenges, and Future Trends," *IEEE Microw. Mag.*, vol. 16, no. 4, pp. 55-70, May 2015.

[21] E. Schires, P. Georgiou and T. S. Lande, "Vital Sign Monitoring Through the Back Using an UWB Impulse Radar With Body Coupled Antennas," *IEEE Trans. Biomed. Circuits Syst.*, vol. 12, no. 2, pp. 292–302, April 2018.

[22] I. D. Castro, M. Mercuri, A. Patel, R. Puers, C. Van Hoof, and T. Torfs, "Physiological Driver Monitoring Using Capacitively Coupled and Radar Sensors," *Appl. Sci.*, vol. 9, no. 19, pp. 1–15, Sep. 2019.

[23] B. K. Park, O. Boric-Lubecke, and V. M. Lubecke, "Arctangent Demodulation With DC Offset Compensation in Quadrature Doppler Radar Receiver Systems," *IEEE Trans. Microw. Theory Tech.*, vol. 55, no. 5, pp. 1073–1079, May 2007.

[24] C. Li and J. Lin, "Random Body Movement Cancellation in Doppler Radar Vital Sign Detection," *IEEE Trans. Microw. Theory Tech.*, vol. 56, no. 12, pp. 3143–3152, Dec. 2008.

[25] A. D. Droitcour, O. Boric-Lubecke, V. M. Lubecke, J. Lin, and G. T. A. Kovacs, "Range correlation and I/Q performance benefits in single-chip silicon Doppler radars for noncontact cardiopulmonary monitoring," *IEEE Trans. Microw. Theory Tech.*, vol. 52, no. 3, pp. 838–848, Mar. 2004.

[26] I. Mostafanezhad, E. Yavari and O. Boric-Lubecke, "A low cost simple RF front end using time-domain multiplexing for direction of arrival estimation of physiological signals," in *IEEE MTT-S Int. Microw. Symp. Dig.*, Jun. 2013, pp. 1–4.

[27] S. Kim and C. Nguyen, "On the development of a multifunction millimeter-wave sensor for displacement sensing and low-velocity measurement," *IEEE Trans. Microw. Theory Tech.*, vol. 52, no. 11, pp. 2503–2512, Nov. 2004.

[28] M. Mercuri, Y.-H. Liu, I. Lorato, T. Torfs, A. Bourdoux and C. Van Hoof, "Frequency-Tracking CW Doppler Radar Solving Small-Angle Approximation and Null Point Issues in Non-Contact Vital Signs Monitoring," *IEEE Trans. Biomed. Circuits Syst.*, vol. 11, no. 3, pp. 671–680, Jun. 2017.

[29] M. Mercuri, Y.-H. Liu, I. Lorato, T. Torfs, F. Wieringa, A. Bourdoux, and C. Van Hoof, "A Direct Phase-Tracking Doppler Radar Using Wavelet Independent Component Analysis for Non-Contact Respiratory and Heart Rate Monitorin," *IEEE Trans. Biomed. Circuits Syst.*, vol. 12, no. 3, pp. 632–643, Apr. 2018.

[30] M. Tang, F. Wang and T. Horng, "Single Self-Injection-Locked Radar With Two Antennas for Monitoring Vital Signs With Large Body Movement Cancellation," *IEEE Trans. Microw. Theory Tech.*, vol. 65, no. 12, pp. 5324–5333, Dec. 2017.

[31] M. Mercuri, D. Schreurs and P. Leroux, "Optimised waveform design for radar sensor aimed at contactless health monitoring," *Electron. Lett.*, vol. 48, no. 20, pp. 1255–1257, Sep. 2018.

[32] M. Mercuri, P.J. Soh, G. Pandey, P. Karsmakers, G.A.E. Vandenbosch, P. Leroux, and D. Schreurs, "Analysis of an Indoor Biomedical Radar-Based System for Health Monitoring," *IEEE Trans. Microw. Theory Tech.*, vol. 61, no. 5, pp. 2061–2068, May. 2013.

[33] W. Su, M. Tang, R. E. Arif, T. Horng and F. Wang, "Stepped-Frequency Continuous-Wave Radar With Self-Injection-Locking Technology for Monitoring Multiple Human Vital Signs," *IEEE Trans. Microw. Theory Tech.*, vol. 67, no. 12, pp. 5396–5405, Dec. 2019.

[34] G. Sacco, E. Pittella, E. Piuzzi, and S. Pisa, "A Radar System for Indoor Human Localization and Breath Monitoring," in *2018 IEEE International Symposium on Medical Measurements and Applications (MeMeA)*, pp. 1–6, Jun. 2018.

[35] G. Sacco, E. Piuzzi, E. Pittella, and S. Pisa, "An FMCW radar for localization and vital signs measurement for different chest orientations," in *Sensors*, vol.20, Jun.2020.

[36] G. Wang, J. Muñoz-Ferreras, C. Gu, C. Li and R. Gómez-García, "Application of Linear-Frequency-Modulated Continuous-Wave (LFMCW) Radars for Tracking of Vital Signs," *IEEE Trans. Microw. Theory Techn.*, vol. 62, no. 6, pp. 1387–1399, Jun. 2014.

[37] M. Mercuri, Y.-H. Liu, S. Sheelavant, S. Polito, T. Torfs and C. Van Hoof, "Digital Linear Discrete FMCW Radar for Healthcare Applications," in *IEEE MTT-S Int. Microw. Symp. Dig.*, Jun. 2019, pp. 144–147.

[38] Liu *et al.*, "9.3 A680 μW Burst-Chirp UWB Radar Transceiver for Vital Signs and Occupancy Sensing up to 15m Distance," in *IEEE ISSCC Dig. Tech Papers*, Feb. 2019, pp. 166–167.

[39] Y. Liu, S. Sheelavant, M. Mercuri, P. Mateman and M. Babaie, "An Ultralow Power Burst-Chirp UWB Radar Transceiver for Indoor Vital Signs and Occupancy Sensing in 40-nm CMOS," *IEEE Solid-State Circuits Lett.*, vol. 2, no. 11, pp. 256–259, Nov. 2019.

[40] M. Mercuri, I. R. Lorato, Y.-H. Liu, F. Wieringa, C. Van Hoof, and T. Torfs, "Vital-sign monitoring and spatial tracking of multiple people using a contactless radar-based sensor," *Nat. Electron.*, vol. 2, pp. 252–262, Jun. 2019.

[41] H. Rohling and C. Moller, "Radar waveform for automotive radar systems and applications," in *IEEE Radar Conf.*, May 2008, pp. 1–4.

[42] J. Wang, T. Karp, J. Muñoz-Ferreras, R. Gómez-García and C. Li, "A Spectrum-Efficient FSK Radar Technology for Range Tracking of Both Moving and Stationary Human Subjects," *IEEE Trans. Microw. Theory Techn.*, vol. 67, no. 12, pp. 5406–5416, Dec. 2019.

[43] Y. S. Koo, L. Ren, Y. Wang and A. E. Fathy, "UWB MicroDoppler Radar for human Gait analysis, tracking more than one person, and vital sign detection of moving persons," in *IEEE MTT-S Int. Microw. Symp. Dig.*, June 2013, pp. 1–4.

[44] N. Andersen *et al.*, "A 118-mW Pulse-Based Radar SoC in 55-nm CMOS for Non-Contact Human Vital Signs Detection," *IEEE J. Solid-State Circuits*, vol. 52, no. 12, pp. 3421–3433, Dec. 2017.

[45] S. Wang *et al.*, "A novel ultra-wideband 80 GHz FMCW radar system for contactless monitoring of vital signs," in *2015 37th Annual International Conference of the IEEE Engineering in Medicine and Biology Society (EMBC)*, Aug. 2015, pp. 4978–4981.

[46] R. Feger, C. Wagner, S. Schuster, S. Scheiblhofer, H. Jager and A. Stelzer, "A 77-GHz FMCW MIMO Radar Based on an SiGe Single-Chip Transceiver," *IEEE Trans. Microw. Theory Techn.*, vol. 57, no. 5, pp. 10020–1035, May 2009.

[47] L. Huang, X. Wang, M. Huang, L. Wan, Z. Han and Y. Yang, "An Implementation Scheme of Range and Angular Measurements for FMCW MIMO Radar via Sparse Spectrum Fitting," *Electronics*, vol. 9, no. 389, pp. 1–15, Feb. 2020.

[48] X. Wang, W. Wang, J. Liu, X. Li and J. Wang, "A sparse representation scheme for angle estimation in monostatic MIMO radar," *Signal Processing*, vol. 104, pp. 258–263, Nov. 2014.

[49] L. Wan, X. Kong and F. Xia, "Joint Range-Doppler-Angle Estimation for Intelligent Tracking of Moving Aerial Targets," *IEEE Internet Things J.*, vol. 5, no. 3, pp. 1625–1636, Jun. 2018.

[50] Z. Fang *et al.*, "Wide Field-of-View Locating and Multimodal Vital Sign Monitoring Based on X-Band CMOS-Integrated Phased-Array Radar Sensor," *IEEE Trans. Microw. Theory Techn.*, vol. 68, no. 9, pp. 4054–4065, Sep. 2020.

[51] F. Wang, F. Zhang, C. Wu, B. Wang and K. J. R. Liu, "ViMo: Multi-person Vital Sign Monitoring using Commodity Millimeter Wave Radio," *IEEE Internet Things J.*, Early Access.

[52] M. Longbrake, "True time-delay beamsteering for radar," in *2012 IEEE National Aerospace and Electronics Conference (NAECON)*, Jul. 2012, pp. 246–249.

[53] O. Kwon *et al.*, "Electrocardiogram Sampling Frequency Range Acceptable for Heart Rate Variability Analysis," *Healthc. Inform. Res.*, vol. 24, no. 3, pp. 198–206, Jul. 2018.

[54] F. Khan and S. H. Cho, "A Detailed Algorithm for Vital Sign Monitoring of a Stationary/Non-Stationary Human through IR-UWB Radar," *Sensors*, vol. 17, no. 2, pp. 1–15, Feb. 2017.

[55] G. Wang, C. Gu, T. Inoue and C. Li, "A Hybrid FMCW-Interferometry Radar for Indoor Precise Positioning and Versatile Life Activity Monitoring," *IEEE Trans. Microw. Theory Techn.*, vol. 62, no. 11, pp. 2812–2822, Nov. 2014.

[56] A. Hommes, A. Shoykhetbrod and N. Pohl, "A fast tracking 60 GHz Radar using a frequency scanning antenna," *2014 39th International Conference on Infrared, Millimeter, and Terahertz waves (IRMMW-THz)*, Sep. 2014, pp. 1–2.

[57] A. Shoykhetbrod, T. Geibig, A. Hommes, R. Herschel and N. Pohl, "Concept for a fast tracking 60 GHz 3D-radar using frequency scanning antennas," *2016 41st International Conference on Infrared, Millimeter, and Terahertz waves (IRMMW-THz)*, Sep. 2016, pp. 1–3.

[58] T. Geibig, A. Shoykhetbrod, A. Hommes, R. Herschel and N. Pohl, "Compact 3D imaging radar based on FMCW driven frequency-scanning antennas," *2016 IEEE Radar Conference (RadarConf)*, May 2016, pp. 1–5.

[59] A. Orth, P. Kwiatkowski and N. Pohl, "A Novel Approach for a MIMO FMCW Radar System with Frequency Steered Antennas for 3D Target Localization," *2019 16th European Radar Conference (EuRAD)*, Oct. 2019, pp. 37–40.

[60] Y. Alvarez-Lopez, C. Garcia-Gonzalez, C. Vazquez-Antuna, S. Ver-Hoeye and F. Las Heras Andres, "Frequency Scanning Based Radar System," *Progress In Electromagnetics Research*, vol. 132, pp. 275–296, Jan. 2012.

[61] P. S. Hall, "Microstrip linear array with polarisation control," *IEE Proceedings H (Microwaves, Optics and Antennas)*, vol. 130, no. 3, pp. 215-224, Apr. 1983.

[62] P. S. Hall, "Microstrip Linear Array for Polarisation-Agile Antenna Applications," in *1981 11th European Microwave Conference*, Sep. 1981, pp. 813–818.

[63] S. Nishimura, K. Nakano and T. Makimoto, "Franklin type microstrip line antenna," in *1979 Antennas and Propagation Society International Symposium*, Jun. 1979, pp. 134–137.

[64] J. Henriksson, K. Markus and M. Tiuri, "A Circularly Polarized Traveling-Wave Chain Antenna," in *1979 9th European Microwave Conference*, Sep. 1979, pp. 174–178.

[65] M. Weenk, H. van Goor, M. van Acht, L. Engelen, T. H. de Belt and S. J. H Bredie, "A smart all-in-one device to measure vital signs in admitted patients," *PloS*, vol. 13, pp. 1-12, Feb. 2018.

[66] S. Nahar, T. Phan, F. Quaiyum, L. Ren, A. E. Fathy and O. Kilic, "An Electromagnetic Model of Human Vital Signs Detection and Its Experimental Validation," *IEEE J. Emerg. Sel. Topics Circuits Syst.*, vol. 8, no. 2, pp. 338–349, Jan. 2018.

[67] F. Adib, H. Mao, Z. Kabelac, D. Katabi and R. C. Miller, "Smart Homes that Monitor Breathing and Heart Rate," in *Proceedings of the 33rd Annual ACM Conference on Human Factors in Computing Systems (CHI '15)*, Apr. 2015, pp. 837–846.

[68] L. Anitori, A. de Jong and F. Nennie, "FMCW radar for life-sign detection," in *2009 IEEE Radar Conference*, May 2009, pp. 1–6.

[69] H. Lee, B.-H. Kim, J.-K. Park and J.-G. Yook, "A Novel Vital-Sign Sensing Algorithm for Multiple Subjects Based on 24-GHz FMCW Doppler Radar," *Remote Sens.*, vol. 11, no. 10, pp. 1-15, May 2019.

[70] S. M. M. Islam, E. Yavari, A. Rahman, V. M. Lubecke and O. Boric-Lubecke, "Multiple Subject Respiratory Pattern Recognition and Estimation of Direction of Arrival using Phase-Comparison Monopulse Radar," in *2019 IEEE Radio and Wireless Symposium (RWS)*, May 2019, pp. 1–4.

[71] Z. Yang, P. H. Pathak, Y. Zeng, X. Liran and P. Mohapatra, "A Circularly Polarized Traveling-Wave Chain Antenna," in *Proceedings of the 17th ACM International Symposium on Mobile Ad Hoc Networking and Computing*, Jul. 2016, pp. 211–220.